$$C_3(\Theta^2\Theta')' = -\frac{C_2}{S^2}F^2\Theta^3 + \frac{C_1}{S}F\Theta^2, \tag{54}$$

where S is the nondimensional shear rate,

$$S \equiv \frac{\Omega(r)\,d}{\nu_0\sqrt{T_0(r)}}, \tag{55}$$

and

$$C_1 \equiv 3\alpha \sin 2\chi, \tag{56}$$

$$C_2 \equiv \frac{6\varepsilon^*(2-\varepsilon^*)}{\pi^{3/2}}\,\mathrm{tr}(\mathbf{A}), \tag{57}$$

$$C_3 \equiv \frac{5\pi^{1/2}(1-2\beta)(5-4\beta)}{(2-\varepsilon^*)M_{zz}}, \tag{58}$$

with

$$\cos 2\chi = \frac{5\alpha}{3(1+\beta)}, \tag{59}$$

$$\alpha \doteq \frac{\sqrt{5\varepsilon^*}}{2}, \quad \beta \doteq \frac{5\varepsilon^*}{14}, \tag{60}$$

and

$$\mathrm{tr}(\mathbf{A}) \doteq \frac{2\pi}{35}\left(70 + 7\alpha^2 + 21\beta^2 - 2\alpha^2\beta + \frac{\alpha^4}{4}\right). \tag{61}$$

Upon integrating (54) over the ring thickness, we obtain

$$S = \frac{C_2}{C_1}\frac{1}{J}, \tag{62}$$

where

$$J \equiv \int_0^\infty F\Theta^2\,d\xi \left(\int_0^\infty F^2\Theta^3\,d\xi\right)^{-1}. \tag{63}$$

With (63), we may employ Eq. (36) to solve for S in terms of J and to write (54) as

$$\Theta'' = -\frac{2(\Theta')^2}{\Theta} + BJF(JF\Theta - 1), \tag{64}$$

where

$$B \equiv -\frac{C_1^2}{C_2C_3} \tag{65}$$

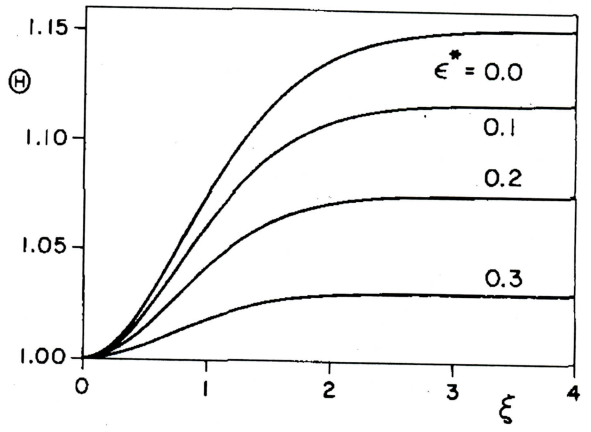

FIG. 1. Dimensionless temperature distribution Θ versus nondimensional axial distance ξ for different values of ε^*. As $\varepsilon^* \to 0.3688$, $\Theta \to 1$.

is positive for all values of ε^*. The introduction of the integral parameter J permits us to easily impose the condition that the heat flux vanishes at large ξ and also removes the quantity S from the equations. This is an advantage because J remains finite for all values of ε^*, while S increases without bound as ε^* approaches the value at which $\sin 2\chi = 0$. In the course of solving for the density and temperature profiles, J is determined iteratively.

The boundary conditions at the midplane are

$$\Theta(0) = 1, \quad \Theta'(0) = 0, \quad \text{and} \quad F(0) = 1. \tag{66}$$

Equations (53) and (64) have been solved subject to the boundary conditions (66) using a Runge–Kutta method beginning with an initial guess for J. Once the profile is determined, J is recalculated using (63) and the integrations of (53) and (64) are repeated. This procedure requires only a few iterations to converge.

Typical profiles for Θ and F are shown in Figs. 1 and 2 for different values of ε^*. In all cases, the temperature increases with distance from the midplane, reaching a constant value as ξ becomes very large. The largest such temperature occurs in the mathematical, but not physical, limit of perfectly elastic collisions; it is about 15% larger than the temperature on the midplane. For $\varepsilon^* = 0.3688$, the temperature is constant throughout. From Fig. 2 it can be seen that the density profiles do not vary appreciably for different ε^* and are close to the isothermal profile:

$$F^* = \exp\left[-\frac{\xi^2}{2(1-2\beta)}\right]. \tag{67}$$

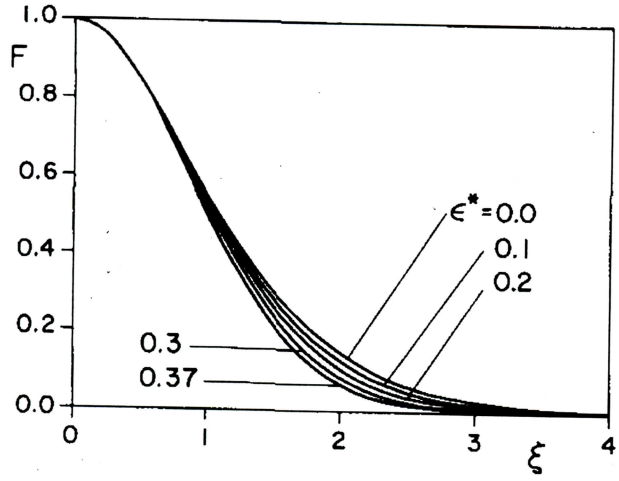

FIG. 2. Dimensionless density distribution F versus nondimensional axial distance ξ for different values of ε^*. The isothermal density profile corresponds to $\varepsilon^* = 0.3688$.

Finally, Fig. 3 shows a detailed energy balance for $\varepsilon^* = 0.1$, with production (P), dissipation (D), and conduction (C) defined by

$$P = BJF\Theta^2, \quad D = BJ^2F^2\Theta^3, \quad \text{and} \quad C = \Theta^2\Theta'' + 2\Theta(\Theta')^2. \tag{68}$$

It is seen that production as well as dissipation of kinetic energy is highest at the midplane. The dissipation of energy near the central plane dominates the production, whereas for large axial distances more energy is generated than can be dissipated; therefore, heat is conducted from large axial distances to the central plane.

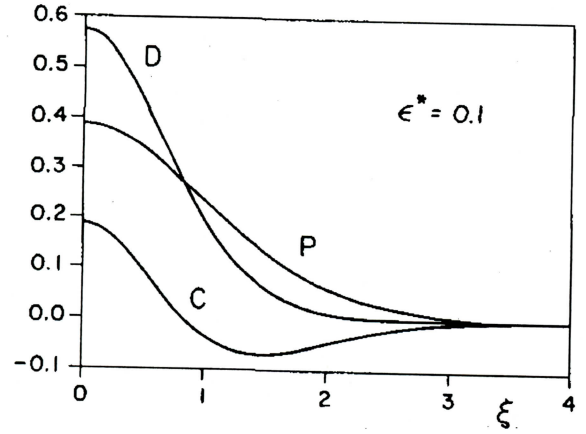

FIG. 3. Energy balance with production (P), dissipation (D), and conduction (C) for $\varepsilon^* = 0.1$ versus nondimensional axial distance ξ.

Of course, the variations of the volume fraction and the granular temperature are determined only relative to their values on the midplane of the ring. In order to determine their midplane values, additional information is required. In the next section, we introduce additional information and solve for these midplane values and the particle diameter.

SATURN'S A-RING

We now give rough estimates of the granular temperature and the solid volume fraction on the midplane and the particle diameter in Saturn's A-ring. As a result of the 6/7 Lindblad resonance, there is a torque $T_{6/7}$ exerted at the outer edge of the A-ring. We first equate this torque to the moment of the integrated shear stress,

$$T_{6/7} = 4\pi R_A^2 \int_0^\infty \rho K_{r\varphi}\, dz, \tag{69}$$

where R_A is the outer radius of the A-ring, $R_A = 1.37 \times 10^8$ m. We define the surface mass density Σ by

$$\Sigma \equiv 2\int_0^\infty \rho\, dz, \tag{70}$$

and use the fact that $\Sigma \doteq 300$ kg m^{-2} and $T_{6/7}/\Sigma \doteq 1.13 \times 10^{11}$ m^4 sec^{-2} (Cuzzi *et al.*, 1984).

Then, upon writing $K_{r\varphi} = T\,\alpha \sin 2\chi$ and using the variables of the previous section in (69) and (70), we have that the midplane temperature and the midplane volume fraction are given by

$$T_0 = \frac{T_{6/7}}{2\pi\Sigma R_A^2}\frac{1}{\alpha \sin 2\chi}\int_0^\infty F\, d\xi \left(\int_0^\infty F\Theta^2\, d\xi\right)^{-1} \tag{71}$$

and

$$\nu_0 = \frac{\Sigma\Omega}{2\rho_s\sqrt{T_0}}\left(\int_0^\infty F\, d\xi\right)^{-1}. \tag{72}$$

Recalling the definition (55), the particle diameter is given in terms of these by

$$d = \frac{S\nu_0\sqrt{T_0}}{\Omega}, \tag{73}$$

where S is given in terms of J by (62). When these quantities are evaluated on the numerical solutions for F and Θ, their values are determined as functions of ε^*.

It is, perhaps, more convenient to have these quantities given as functions of the optical depth τ defined by

$$\tau \equiv \frac{3}{d}\int_0^\infty \nu\, dz = \frac{3}{S}\int_0^\infty F\, d\xi = 3\frac{C_1}{C_2}J\int_0^\infty F\, d\xi. \tag{74}$$

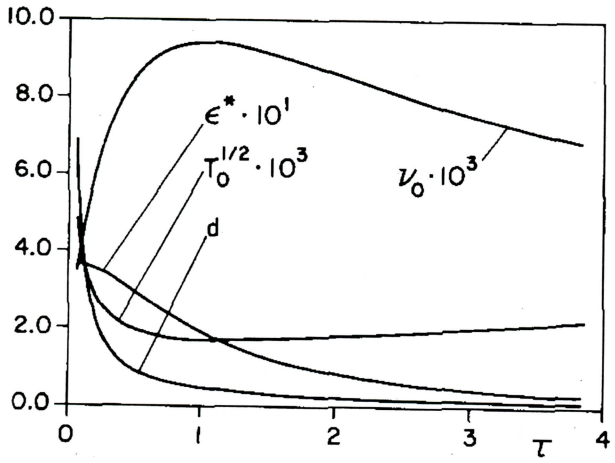

FIG. 4. The quantities $\sqrt{T_0}$ (m sec^{-1}), ν_0, d(m), and ε^* versus τ.

Because (74) relates τ and ε^* on solutions, this is easy to do. The graphs of T_0, ν_0, d, and ε^* versus τ are shown in Fig. 4.

The relationship between ε^* and τ that results is essentially identical to the relationships between ε^* and τ determined by Goldreich and Tremaine (1978) and Araki (1991). That is, the variation of temperature normal to the plane of the ring does not have a discernible effect on the relationship between the optical depth and the coefficient of restitution. We can take advantage of this lack of sensitivity to the variation of the granular temperature normal to the ring to obtain simple approximate forms of (71)–(73) that are more amenable to physical interpretation.

If we take the temperature to be uniform and use the isothermal density distribution (67) in the integrals (71) and (72), the relation corresponding to (71) is clearly a determination of the midplane value of $K_{r\varphi}$ that has been solved for T_0:

$$T_0 = \frac{T_{6/7}}{2\pi\Sigma R_A^2}\frac{1}{\alpha \sin 2\chi}. \tag{75}$$

The quantity $\alpha \sin 2\chi$ is the kinematic viscosity introduced by Goldreich and Tremaine (1978), normalized by $2T_0/3\Omega$. As they show, this normalized kinematic viscosity first increases with τ and then decreases. The minimum in the curve of T_0 versus τ in Fig. 4 is a consequence of this. In the same limit, (72) becomes a relation between the midplane value of K_{zz} and ν_0:

$$\nu_0 = \frac{\Sigma\Omega}{\rho_s\sqrt{2\pi}}\frac{1}{\sqrt{T_0(1-2\beta)}}. \tag{76}$$

Because β is a monotone increasing function of ε^*, the maximum in the curve of ν_0 versus τ is inherited from the minimum in the curve of T_0 versus τ. The particle diameter then follows from (73) with $J = \sqrt{2}$, and the optical depth is

$$\tau = \frac{3\pi^2\alpha \sin 2\chi}{2\varepsilon^*(2-\varepsilon^*)\,\mathrm{tr}(\mathbf{A})}\sqrt{1-2\beta}. \tag{77}$$

Upon employing (59)–(61), these may be expressed in terms of ε^* alone.

It is interesting that the introduction of so modest an amount of information permits such explicit predictions to be made of the midplane volume fraction, the midplane granular temperature, and the particle diameter in the context of this simple model of the ring.

ACKNOWLEDGMENTS

The authors have benefitted from conversations with J. A. Burns. They are also indebted to C. Zhang for his assistance with the energy flux. Finally, they are grateful to S. Araki for suggestions that led to the improvement of the manuscript. This work was begun when Volker Simon was an exchange student at Cornell University. He is pleased to thank F. G. Kollmann and W. H. Sachse, who initiated this exchange program and thereby laid the foundation for the current collaboration. He is also appreciative of the hospitality shown to him during visits to the Department of Theoretical and Applied Mechanics, Cornell University, in the summers of 1988 and 1989. These visits were supported by the U.S. Army Research Office through the Mathematical Sciences Institute at Cornell University.

REFERENCES

Araki, S., and S. Tremaine 1986. The dynamics of dense particle disks. *Icarus* **65**, 83–109.

Araki, S. 1988. The dynamics of particle disks. II. Effects of spin degrees of freedom. *Icarus* **76**, 182–198.

Araki, S. 1991. The dynamics of particle disks. III. Dense and spinning particle disks. *Icarus* **90**, 139–171.

Cuzzi, J. N., J. J. Lissauer, L. W. Esposito, J. B. Holberg, E. A. Marouf, G. L. Tyler, and A. Boischot 1984. Saturn's rings: Properties and processes. In *Planetary Rings* (R. J. Greenberg and A. Brahic, Eds), pp. 73–200.

Goldreich, P., and S. Tremaine 1978. The velocity dispersion in Saturn's rings. *Icarus* **34**, 227–239.

Jenkins, J. T., and M. W. Richman 1988. Plane simple shear of smooth inelastic circular disks: The anisotropy of the second moment in the dilute and dense limits. *J. Fluid Mech.* **192**, 313–328.

Richman, M. W. 1989. The source of second moment in dilute granular flows of highly inelastic spheres. *J. Rheol.* **33**, 1293–1306.

Shuhkman, G. 1984. Collisional dynamics of particles in Saturn's rings. *Astron. Zh.* **61**, 985–1004; translated in *Sov. Astron.* **28**, 547–585.

Stewart, G. R., D. N. C. Lin, and P. Bodenheimer, 1984. Collision induced transport processes in planetary rings. In *Planetary Rings* (R. J. Greenberg and A. Brahic, Eds.), pp. 447–512.

Zhang, C. 1993. *Kinetic Theory for Rapid Granular Flows*, Ph.D. Dissertation, Cornell University, Ithaca, NY.